pubs.acs.org/Biomac

Article

Effects of Thermal Aging on the Adhesion Forces of Biopolymers of Wood Cell Walls

Juan Li* and Bohumil Kasal*

Cite This: *Biomacromolecules* 2022, 23, 1601−1609

Read Online

ACCESS | Metrics & More | Article Recommendations

ABSTRACT: Wood is the most important, industrially used renewable resource on the planet, but the aging mechanism of biopolymers on cell walls is poorly understood. Adhesion properties are of critical importance for wood and many other lignocellulosic materials. We used atomic force microscopy and defined the jump-off force ratio in the retract force−displacement curve to study the adhesion force phenomenon and the effects of heat treatments. Here, we identified two sigmoidal curves describing the shift of the adhesion force and the jump-off force ratio: the first curve was attributed to the movement of extractives and the second to the degradation of the hemicellulose−lignin matrix. We confirmed the hypothesis formulated in this paper by the cell wall surface topography, the analysis of the treated samples by Fourier transform infrared spectroscopy, and the analysis of volatiles during heating by headspace gas chromatography-mass spectrometry.

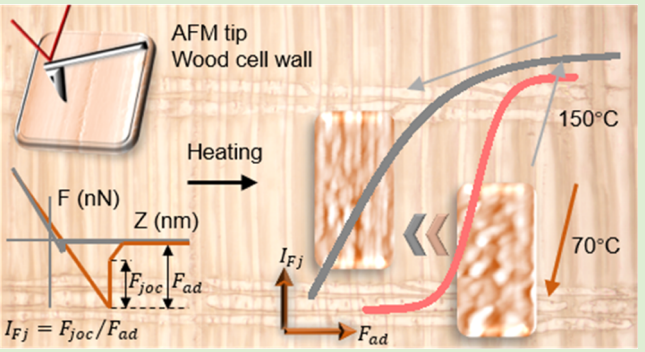

INTRODUCTION

Aging is defined as irreversible changes of properties of interest, under the effect of various factors, such as temperature, moisture, loading, UV light, or chemical solutions in time. We are interested in the effect of aging factors (specifically, temperature) on the surface of wood cell walls. We study wood because of its increasing importance as a structural material and the lack of understanding of the in situ aging processes. The temperature influences almost every aging process in manufacturing and application of wood ranging from wood composite manufacturing to the use of wood in construction. Heat is often used as a vehicle to accelerate the aging processes of polymers, such as the application of time−temperature superposition.[1−6] For the wood material, aging under dry conditions at ambient temperature is mainly a mild oxidation process.[7,8] Heat treatments at 100−150 °C were used to accelerate the oxidation process and to avoid dissimilar chemical reactions under natural aging.[8−16] However, the detailed mechanism of thermal oxidation is rarely addressed.[8]

Wood is a cellular structure composed of biopolymers: cellulose, hemicelluloses, lignin, and small portions of other substances, such as extractives. Several studies used atomic force microscopy (AFM) to visualize the ultrastructure of the cell wall on transverse cross sections.[17−21] Some studies used adhesion forces from force−displacement curves to characterize the wood fine structure nanomechanically[17,22,23] and to detect whether adhesion forces on wood surfaces changed with UV light or heat.[24−27] However, the interpretation of the adhesion force measurements is limited, at best. This gap is mainly due to the structural and chemical heterogeneity of natural wood surfaces, the lack of reliable repositioning techniques, and the small sample sizes, which prevents drawing statistically significant conclusions. In the previous study, we proposed a systematic and reliable repositioning method,[28] which is a key in studying heterogeneous surfaces of plants such as wood.

The force−displacement curve shows two discontinuities: a jump-to-contact and a jump-off-contact. These jumps are due to the inherent stiffness of the tip, the stiffness of the cantilever, and the force gradient between the tip and sample.[29] Researchers have studied the jumps: jump distances, material structural transformation, and tip−sample force changes.[30−34] For example, the atoms in gold samples formed a neck to adhere to the tip.[30,33]

We believe that the jumps contain material information and can help measure material changes in the complex wood cell wall system during the aging process. Given the identical tip and cantilever stiffness, the jumps reflect the nature of the force gradient between the tip and the material, thus relating to the

Received: October 26, 2021
Revised: February 15, 2022
Published: March 18, 2022

https://doi.org/10.1021/acs.biomac.1c01397
Biomacromolecules 2022, 23, 1601−1609

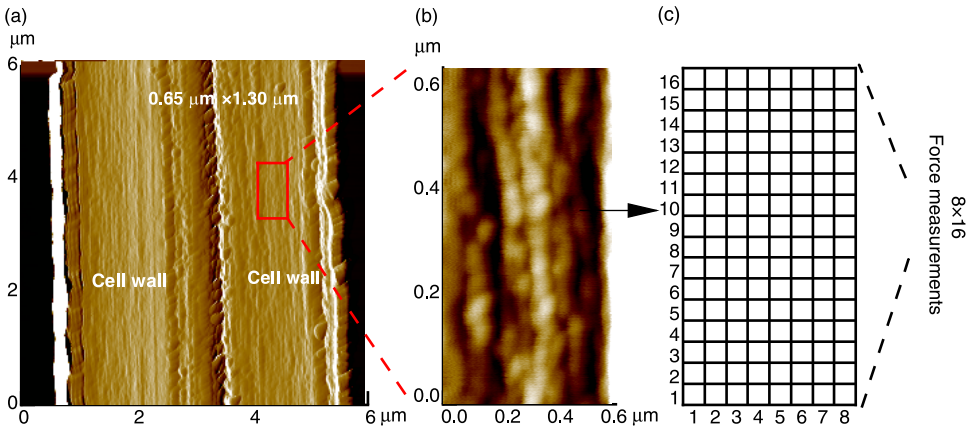

Figure 1. Diagram of AFM adhesion force measurements. (a) Topography of two adjacent cell walls and a selected area in the red rectangle. (b) Magnification of the selected area. (c) Measurement points using the force−volume mode.

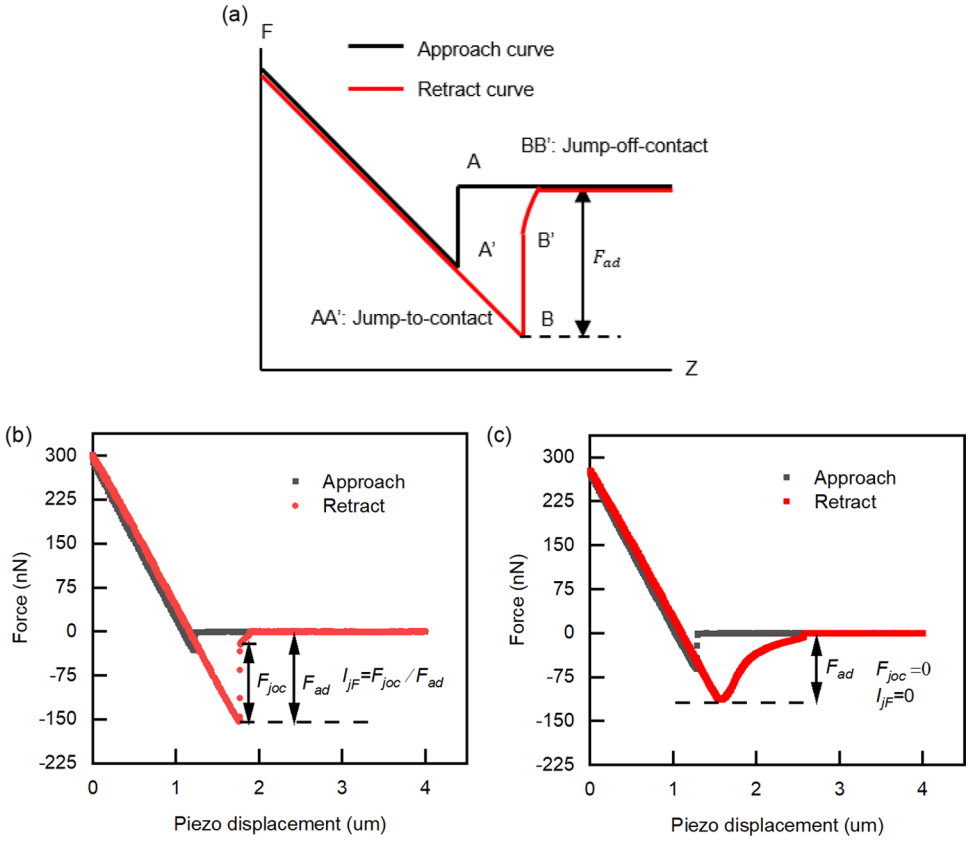

Figure 2. Force−displacement curve. (a) Two jumps—AA′: jump-to-contact and BB′: jump-off-contact. (b) Discontinuous "jump-off-contact": $I_{jF} = \frac{F_{joc}}{F_{ad}}$. (c) Continuous separation: $I_{jF} = 0$.

material properties. Instead of focusing on the jump distance, we define the jump-off force ratio in the retract force−displacement curve.

We asked (a) whether AFM adhesion force measurements could describe the aging of wood cell wall surfaces; (b) whether the jump-off force ratio in the retract force−displacement curve helped identify different chemical components; and (c) whether migrating extractives affected the adhesion force measurements.

METHODS

Materials. Norway spruce (Picea abies) wood samples with dimensions of 3 mm × 3 mm × 5 mm [radial (R) × tangential (T) × longitudinal (L)] were cut from an air-dried woodblock with dimensions of 8 mm × 5 mm × 50 mm (R × T × L) with a stainless-steel razor blade. Ten samples were randomly selected for the AFM measurements, and the radial surfaces were polished with a diamond knife (histo DH4560, Diatome Ltd, Switzerland) using a rotary microtome (HM 360, Microm, Germany). The polished samples were fixed on the AFM sample holder with double-sided tape. The wood samples in the natural state were stored in a desiccator [relative humidity (RH) < 10%, 21 ± 2 °C] for at least 1 week for stabilization. Wood slices with a tangential thickness of about 100 μm were cut from randomly selected samples with the same microtome.

Selection of Treatment Temperature. Based on the literature review,[9−11] the temperature of 150 °C was selected as the aging acceleration factor, expecting to cause measurable changes in the major

https://doi.org/10.1021/acs.biomac.1c01397
Biomacromolecules 2022, 23, 1601−1609

wood chemical components within a reasonable time. The presence of extractives inevitably plays a role in the measurements of wood surface properties. Therefore, the thermal treatment was also performed at 70 °C, which induced the migration of extractives toward the surface.[10,35−37]

Treatment. For AFM measurements, three samples were treated in an oven with circulating air at 150 °C for an accumulated time of 6, 24, 51, 72, 144, 240, 384, and 624 h. Another three samples were treated at 70 °C for the same duration. After each treatment, the wood samples were equilibrated in the desiccator (RH < 10%, 21 ± 2 °C) for at least 24 h and then measured by AFM. For Fourier transform infrared (FTIR) spectroscopy measurements, the wood slices were treated at 150 and 70 °C for the accumulated time of 6, 72, 144, 240, 384, and 624 h. After each treatment, the wood samples were equilibrated at 20 °C and 50% RH for 24 h and then measured by FTIR spectroscopy.

Repositioning of the AFM Tip. Identical samples were treated and measured throughout the entire test, and identical cell wall sections were scanned after each treatment. We have used the repositioning method that we developed and validated.[28]

Atomic Force Microscopy (AFM) Measurements. Adhesion force measurements were conducted with an AFM Agilent Technologies 5500 (Agilent Technologies, Inc., Santa Clara, CA) in an environmental chamber using the force−volume mode. The chamber was continuously supplied with nitrogen, and the relative humidity was below 5%. A silicon Multi75AL-G tip (Nanoandmore, Germany) was first blunted to avoid uncontrolled wear. The force constant of the tip was determined to be 3 N/m using the thermal noise method, and the deflection sensitivity was 100 nm/V. Our preliminary tests showed that a blunt tip used for the natural wood cell walls in the nitrogen gas gave consistent and steady force measurements. A single AFM tip was used to measure identical samples throughout the entire experiment to reduce the variations between tips and between wood samples and wood cell walls. The tip wear was checked frequently using a silicon surface and wood control samples.

The topography image of the cell wall was obtained by scanning in the contact mode (256 × 256 pixels), and a rectangular area with dimensions of 0.65 μm × 1.3 μm on the secondary cell wall was selected. A contact-mode scan was made on the selected area with 256 × 512 pixels. The adhesion force measurements were conducted in the force−volume mode with 8 measurement points on each line and 16 lines in total. One-hundred twenty-eight adhesion force curves were collected on each selected cell wall section (Figure 1).

Force−Displacement Curve. The raw curve obtained by AFM is a force−displacement curve, where the rest position of the cantilever is recorded. The tip−sample distance is the distance after the subtraction of the cantilever deflection from the displacement. In this article, we used the raw curves: force−displacement curves. A force−displacement curve is shown in Figure 2a. The tip approaches the sample (black curve), jumps to contact with the surface, and continues to deform to the predefined load. Then, the tip starts to retract (red curve). When the tip separates from the surface, the adhesion force (F_{ad}) occurs.

In the force−displacement curves, there are two discontinuities (A−A′ and B−B′; see Figure 2a): jump-to-contact in the approach curve and jump-off-contact in the retract curve. The jumps occur when the tip−sample force gradient, dF/dZ, is larger than the cantilever stiffness, k_c. The jump-to-contact first increases with k_c and then decreases; the jump-off-contact always decreases with k_c.[29]

Jump-Off Force Ratio. Instead of the jump distance of the tip in the Z direction, we are interested in the ratio between the jump-off-contact force span (F_{joc}) and the adhesion force (F_{ad}) in the retract force−displacement curve. We define the jump-off force ratio as (Figure 2b)

$$I_{jF} = \frac{F_{joc}}{F_{ad}} \tag{1}$$

where I represents the normalization of the jump-off-contact force span by the adhesion force so that I_{jF} lies between 0 and 1. We observed that some force−displacement curves had no discontinuities when the tip retracted away from the sample surface, and, in this case, the jump-off ratio (I_{jF}) was set to zero (Figure 2c).

We used the jump-off force ratio to identify the chemical components on the surface of wood samples subjected to heat treatments.

Fourier Transform Infrared (FTIR) Spectroscopy. Fourier transform infrared spectra of the wood samples were measured with a Bruker Tensor 25 FTIR spectrometer equipped with the attenuated total reflection (Bruker Optics, Bremen, Germany). Spectra were collected in the wavenumber range of 4000−400 cm^{-1} with a resolution of 4 cm^{-1} and 32 scans. Three measurements were conducted on each sample. Spectra were baseline corrected and normalized to the highest peak so that the absorbance lies between 0 and 1.

Headspace Gas Chromatography−Mass Spectrometry (GC−MS). Spruce wood sawdust was stored at 20 °C and 65% relative humidity for one year before tests. As shown in Figure 3, 150 mg of sawdust was placed in a 10 mL headspace vial with carried-lined screw caps. Four headspaces with sawdust were stored at room temperature for 10 days, and two headspaces with sawdust were heated in an oven at 150 °C for 10 days. The samples were then equilibrated at 70/150 °C for 6 h in the headspace sampler oven (Agilent Headspace sampler 7697A). The analysis was carried out on the Agilent J&W HP-5MS UI column (I = 30 m, I.D. = 0.32 mm, film = 0.25 μm) using a GC/MS system (Agilent GC/MS 7890A/5975C). Identification was based on spectral libraries (NIST/Wiley).

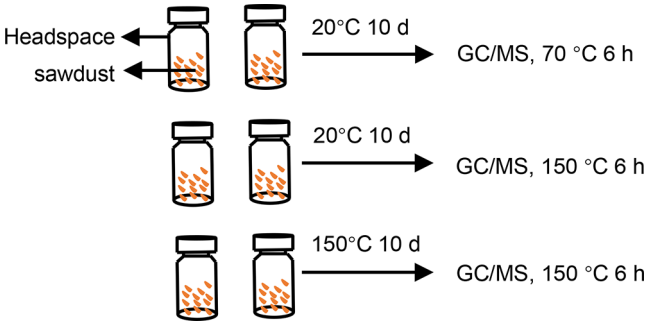

Figure 3. Schematic of headspace GC−MS tests.

Boltzmann's Sigmoidal Equation. Sigmoid functions with the shape of Boltzmann equations have been used frequently to describe diverse biological or medical situations related to transition phenomena, revealing their physical or geometric behaviors.[38] The Boltzmann's sigmoidal equation describes the transition of a dependent variable from one state to another significantly different state as a function of an independent variable.[39] The function has a sigmoid-shaped curve

$$y(x) = y_i - \frac{y_i - y_r}{1 + \exp((x - x_0)/\Delta x)} \tag{2}$$

where y is the dependent variable, x is the independent variable, y_i and y_r are the left and right asymptotes of y, x_0 is the center (where y returns the mean of y_i and y_r), and Δx is the constant period of the independent variable that determines the rise profile or decrease from y_i to y_r (for a high Δx, the increase is slow, and for a low Δx, the increase is fast).

Sample Size. Ten samples were randomly selected and measured by AFM in the natural state, and 5−10 cell walls were chosen on each sample. One-hundred twenty-eight force curves were collected on each cell wall. In total, we measured 73 cell walls and more than 8000 force curves on untreated samples and more than 2000 force curves on the samples treated at 150 and 70 °C.

Data Processing. The calculation of the adhesion force and the jump-off force ratio was performed using a self-written MATLAB code. After discarding outliers, defined as 5% of the lowest and highest ends of the 128 measurement points on each cell wall, each data point (in Figures 4a and 5a) represented the truncated average and variance in adhesion forces and jump-off force ratios (114 data sets). Data were summarized as average ± standard deviation ($\bar{x} \pm s$). The sigmoidal fitting and the descriptive statistics were performed in Origin 2019b.

https://doi.org/10.1021/acs.biomac.1c01397
Biomacromolecules 2022, 23, 1601−1609

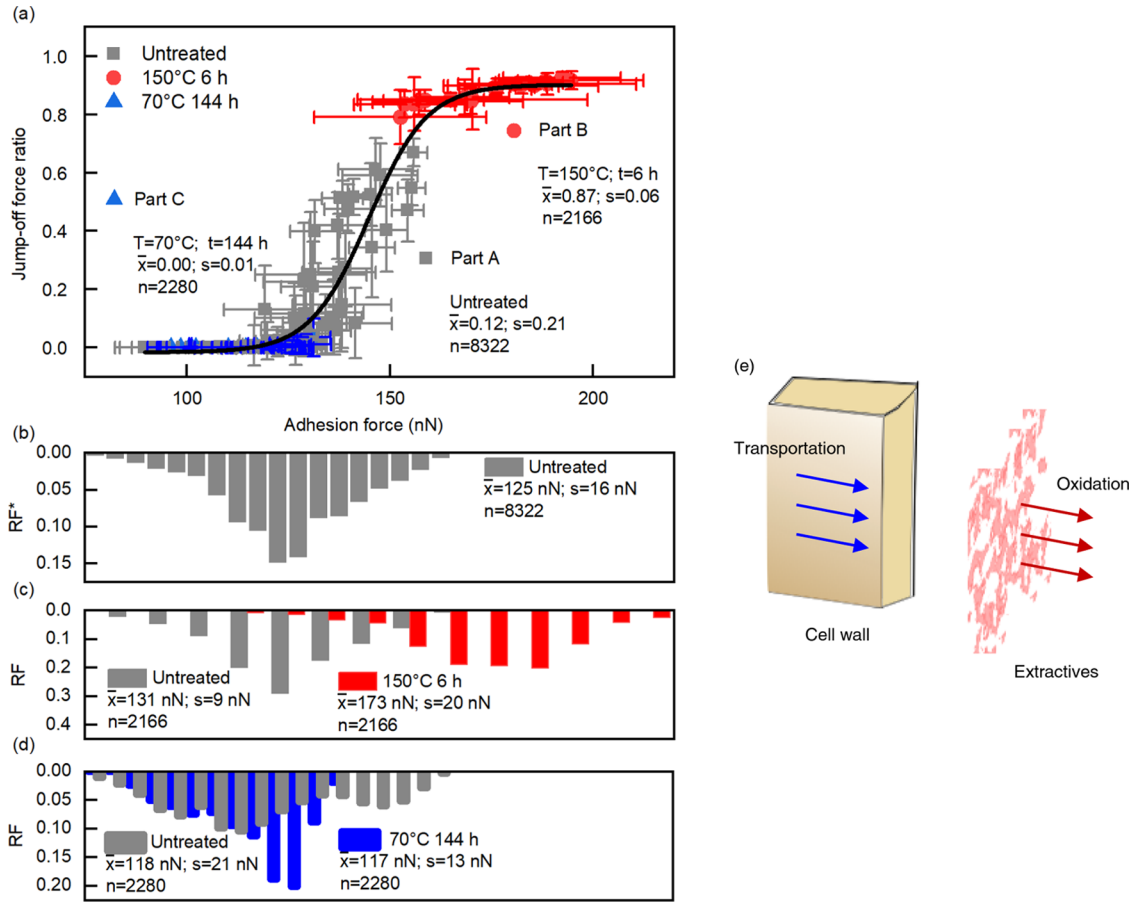

Figure 4. Diagram of the first sigmoidal curve of adhesion force−jump-off force ratio. (a) Heat treatments at 150 °C for 6 h shifted the adhesion forces upward to the top plateau. At 70 °C, the adhesion forces shifted downward to the bottom plateau after 144 h and remained there. (b) Histogram of the adhesion forces of untreated samples. (c) Histogram of adhesion forces of untreated and treated samples [temperature (T) = 150 °C and time (t) = 6 h]. (d) Histogram of adhesion forces of untreated and treated samples (T = 70 °C and t = 144 h). Horizontal axes in panel (b) through panel (d) represent the magnitude of the adhesion forces showed in panel (a). T: temperature; t: time; $\bar{x}$: arithmetic average; s: standard deviation; and n: number of measurements. (e) Diagram of extractive transportation and oxidation. *Relative frequency.

RESULTS

First Sigmoidal Curve. To quantify the spring-back during the AFM tip retraction, we defined the jump-off force ratio in the retract force−displacement curve (Figure 2). We have collected about 8000 data points from 73 cell walls in 10 untreated wood samples (Figure 4a, gray points) and more than 2000 from treated samples (Figure 4a, red and blue points). We used the Boltzmann's equation to describe the sigmoidal curve (Figure 4a, black curve)

$$I_{jF} = 0.9 - \frac{0.9}{1 + \exp((F_{ad} - 144.7)/7.2)} \quad (3)$$

where the adjusted R^2 is 0.94 and the reduced χ^2 is 0.007.

The sigmoidal function indicates that different processes occur as a result of the treatment temperature and time. We identified the upward shift at higher temperatures (150 °C) and downward shift at lower temperatures (70 °C) (see Figure 4a). We hypothesized that the movement of extractives caused the adhesion force and jump-off force ratio to shift, and this shift depended on the temperature level. At lower temperatures (70 °C), the extractives move to the surface but are not fully oxidized, and the transportation rate is higher than the oxidation rate—the extractives accumulate on cell wall surfaces and dominate the adhesion force (Figure 4e). This has been observed by other researchers: the extractives started to transport to the surface in the temperature range of 42−90 °C and disappeared at a temperature more than 200 °C by oxidation.[36] At higher temperatures (150 °C), however, the oxidation rate was higher than the transportation rate, and the concentration of extractives on the surface decreased (Figure 4e). Therefore, the top plateau of the sigmoidal curve represents a near extractive-free surface, where the underlying major chemical components, hemicelluloses, lignin, and cellulose, are exposed. The bottom plateau represents a extractive-abundant surface, and the middle part represents a situation when the adhesion forces are controlled by both the presence of extractives and exposed major wood structural components. This interpretation was based on the literature,[36] and no direct chemical analysis on extractive behavior was performed in this study.

Second Sigmoidal Curve. We found three phases in the adhesion force and jump-off force ratio with a heating time of 24−624 h at 150 °C (Figure 5a): a leftward shift in phase 1, an upward shift in phase 2, and a downward shift in phase 3. We fitted the Boltzmann's equation to the sigmoidal curve (Figure 5a, second curve in blue):

$$I_{jF} = 0.99 - \frac{1.54}{1 + \exp((F_{ad} - 74.9)/26.5)} \quad (4)$$

https://doi.org/10.1021/acs.biomac.1c01397
Biomacromolecules 2022, 23, 1601−1609

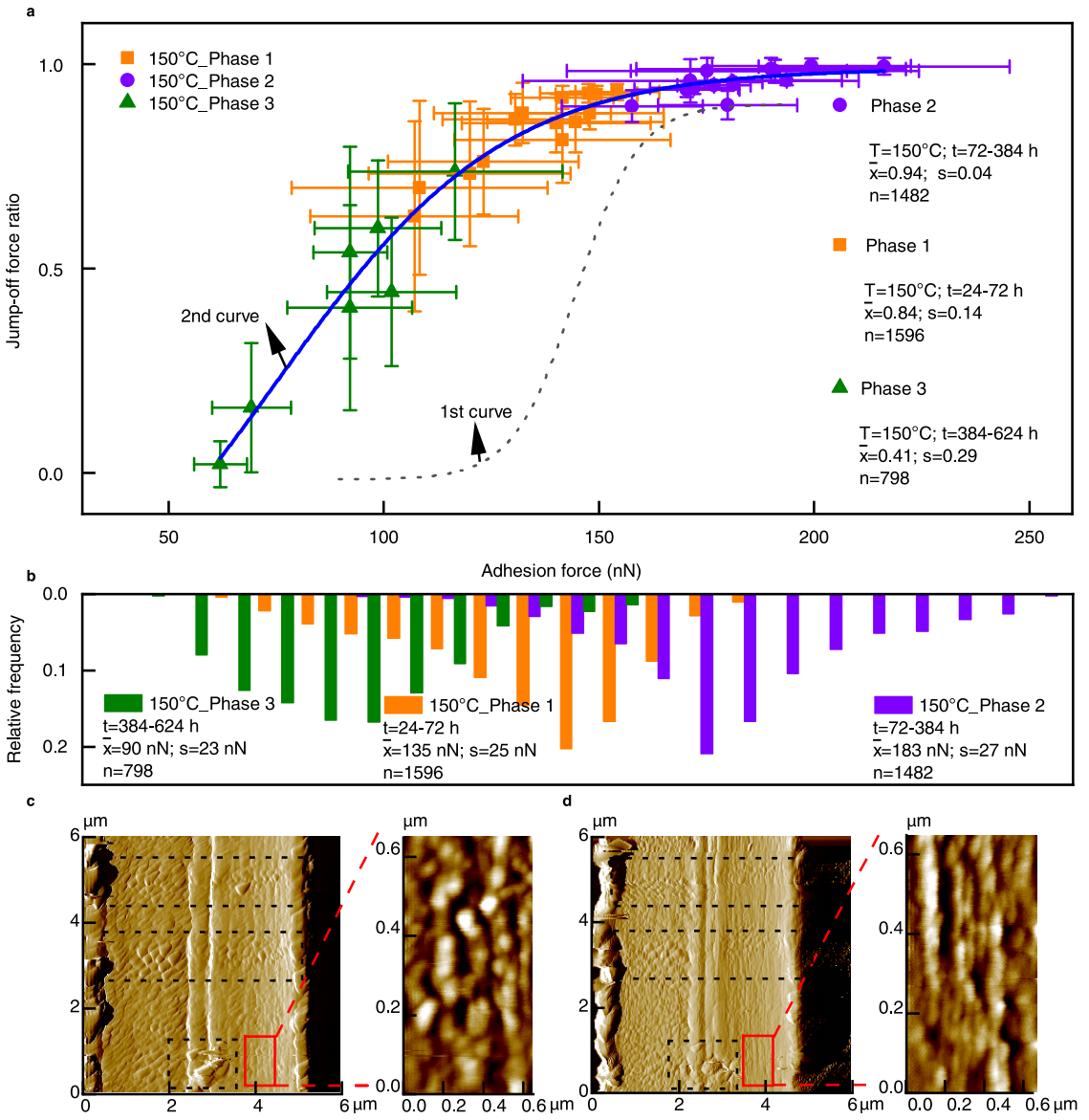

Figure 5. Diagram of the second sigmoidal curve of adhesion force−jump-off force ratio. (a) Data shifting after heating at 150 °C for 24−624 h. (b) Histogram of the adhesion forces from samples treated at 150 °C in phases 1, 2, and 3. (c) Image of the untreated cell wall. (d) Image of the treated cell wall in phase 3. Horizontal axes on panels (b) and (c) represent the magnitude of the adhesion forces shown in panel (a). *T*: temperature; *t*: time; $\bar{x}$: arithmetic average; s: standard deviation; *n*: number of measurements. *Relative frequency.

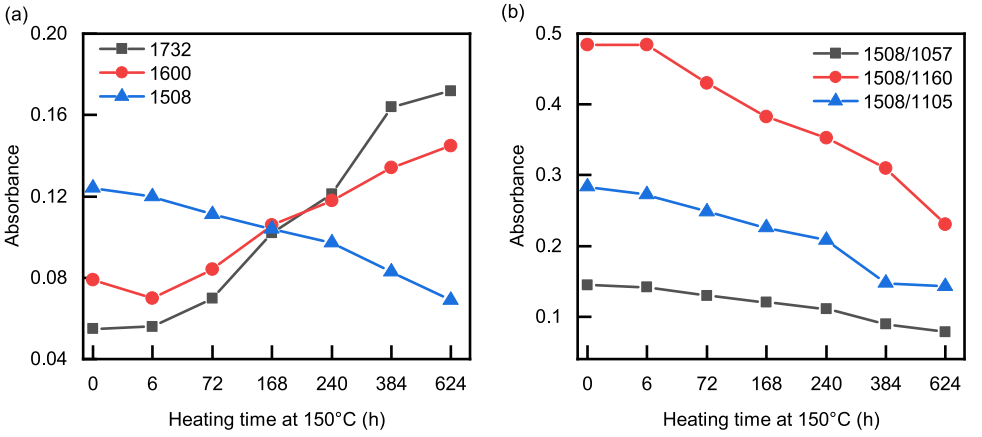

Figure 6. Trend of the intensity of FTIR spectra. (a) Intensity of wavenumbers 1732, 1600, and 1508 cm^{-1}. (b) Intensity of the ratio between 1508 and 1051, 1157, and 1105 cm^{-1}.

https://doi.org/10.1021/acs.biomac.1c01397
Biomacromolecules 2022, 23, 1601−1609

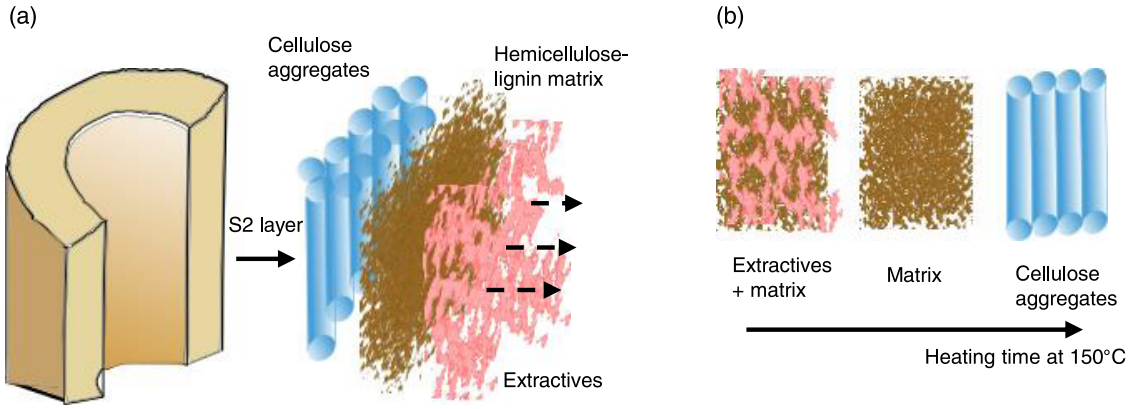

Figure 7. Qualitative model of the thermal aging process. (a) Tracheid cell is cut through by the microtome knife. The exposed cell wall surface is from the outside to the inside: a layer of extractives, a layer of the hemicellulose–lignin matrix, and a layer of cellulose aggregates. The extractives are transported to the surface and oxidized. (b) Dominating chemical components on wood cell surfaces during the thermal treatment at 150 °C: a combination of extractives and the hemicellulose–lignin matrix on an untreated cell wall, the matrix prevails after the extractives degrade, and the cellulose aggregates are exposed after the matrix degrades.

where the adjusted R^2 is 0.97 and the reduced χ^2 is 0.002.

We hypothesized that the hemicellulose–lignin matrix degraded with the heating time at 150 °C and shifted the adhesion forces. We confirmed this hypothesis with the cell wall topography before and after treatments, by Fourier transform infrared (FTIR) spectroscopy and headspace GS-MS.

Topography. We believe that the cellulose aggregates appear on the treated cell wall topography (in phase 3) after the amorphous matrix degrades. We marked some cutting artifacts on the untreated cell wall (black dot circles, see Figure 5c) and found that they disappeared in phase 3 (Figure 5d). The morphology changed from an irregular pattern to regular parallel lines. These lines were 20–60 nm in width, which were comparable to the values for cellulose aggregates reported in the literature: 10–60 nm[40] and, specifically, 10–30 nm with AFM.[19,20] The larger width that we measured was attributed to the widening effect[20] of the blunted tip we used. Therefore, phase 3 means that the cellulose aggregates are exposed gradually when the hemicellulose–lignin matrix is removed with time in phase 1 and phase 2: a removal effect of the heat. The amorphous pattern observed on untreated cell walls (Figure 5c) comes from the extractives and the matrix.

FTIR. FTIR spectra showed the heat oxidized and degraded the hemicellulose–lignin matrix with time at 150 °C. The band between 1700 and 1750 cm^{-1} increased, and the peak shifted from 1732 to 1720 cm^{-1} (Figure 6a). This band represents unconjugated carbonyl groups. Some researchers observed the same trend and suggested lignin condensation at the expense of conjugated carbonyl groups and the opening of the aromatic ring.[41−45] Other researchers reported that the band initially decreased due to the degradation of hemicelluloses and then increased due to the oxidation of lignin and carbohydrates.[43,46] Hemicelluloses degraded first in thermal treatments, where the cleavage of acetyl groups and the released acetic acid further catalyzed the hydrocarbons and lignin to depolymerize.[43]

The band 1508 cm^{-1} decreased continuously (Figure 6a) and was lower in density than the band 1600 cm^{-1} at the treatment time of 384–634 h (Figure 5a, phase 3). The bands around 1500 and 1600 cm^{-1} represent lignin aromatic ring vibrations of guaiacyl and syringyl units, respectively. Softwood has a higher content of guaiacyl units and shows higher intensity in the band at 1500 cm^{-1} than at 1600 cm^{-1}. Researchers reported the same trend and suggested the splitting of aliphatic side chains and the cleavage of β-*O*-4 linkages in lignin structures.[41,43,44,47]

The bands 1160, 1057, and 1105 cm^{-1} for cellulose and hemicelluloses increased and suggested that aliphatic alcohols formed and the content of crystalline cellulose increased after the heat treatments.[42,47] The ratio of the softwood lignin band 1508 cm^{-1} and the carbohydrate band decreased continuously and suggested that the lignin content decreased (Figure 6b). Therefore, the FTIR results confirmed that the hemicellulose–lignin matrix degraded and its content decreased compared with cellulose.

Headspace GC–MS. The volatiles at 70 °C for 6 h are mainly terpenes, which are natural wood extractives. The volatiles at 150 °C for 6 h showed multiple terpenes and the typical degradation products found in the hemicellulose oxidation and pyrolysis: formic acids, acetic acids, furfurals, and furans.[48] It was reported that the 3-*O*-acetyl group in xylan reacted with the hydrogen atom linked to the C2 position to form the carboxyl group. The C6 + acetyl group underwent through a pericyclic reaction to form acetic acid.[49] Xylose was known to convert to furfural and 5-methyl furfural. Vanillin was also detected, indicating the degradation of lignin.

After the wood samples were heated at 150 °C for 240 h, the volatiles showed different products compared with the heating at 150 °C for 6 h. The terpenes were no longer detected, indicating that these volatile extractives might have evaporated during treatments. Approximately five aromatic compounds were detected: vanillin, apocynin, 2-methoxyphenol, 2-methoxy-4-methylphenol, and methyl vanillate, indicating that lignin was oxidized and depolymerized. The low molecular weight aromatic compounds might be formed by dimethoxylation and C_α–C_β breakdown.[50] Acetic acid, propanoic acid, and furfurals indicated the degradation of hemicelluloses. Levoglucosenone has been detected and showed the degradation of cellulose.[51]

Extractives such as terpenes started to move at both 150 and 70 °C, therefore, we can conclude that the downward shift at 70 °C and the upward shift at 150 °C on the first sigmoidal curve are related to the movements of extractives: at 70 °C, the moving speed from the inside to the surface is larger than the evaporating speed, resulting in the extractive accumulation on the surface; at 150 °C, the opposing processes occur, resulting in an extractive-free surface. Similar results were reported by other researchers:

https://doi.org/10.1021/acs.biomac.1c01397
Biomacromolecules 2022, 23, 1601−1609

heat treatments at 120 °C for 10 h reduced the terpenes in the green fir wood by >99%.[52] Hemicelluloses and lignin start to degrade when treated at 150 °C for 6 h and more aromatic degradation products when treated at 150 °C for 10 days indicate that lignin is decomposed with a longer treatment time. Therefore, we can conclude that the second sigmoidal curve indicates the degradation of the hemicellulose−lignin matrix.

DISCUSSION

In this work, we measured more than 8000 points on untreated wood cell walls and more than 2000 points each on treated cell walls by heat treatments at 150 and 70 °C. We used the repositioning method that allowed us to perform pairwise comparisons. We believe that the force gradient in the retract force−displacement curve reflects the nature of the interactions between the tip and the material and define the jump-off force ratio (Figure 2). This permitted us to quantify the mechanism of the AFM tip separation. We found two sigmoidal curves in adhesion force magnitudes and the jump-off force ratios: (1) the first curve indicated the transportation and oxidation processes of extractives during heat treatments and (2) the second curve indicated the degradation process of the hemicellulose−lignin matrix. The cell wall topography, FTIR, and GC−MS results confirmed that the heat treatment removed the top layer substances from wood cell walls: (1) the parallel lines on the treated cell wall topography suggested cellulose aggregates appeared after the matrix degraded; (2) the FTIR analysis revealed that the intensity of carbonyl groups increased, the aromatic ring intensity of softwood lignin decreased, and the lignin to carbohydrate ratio decreased: this means that the hemicellulose−lignin matrix was oxidized and degraded; and (3) the GC−MS analysis showed the acids and furfurals derived from hemicellulose degradation and five aromatic monomers from lignin depolymerization in the volatiles of wood samples when treated at 150 °C for 10 days. Degradation products from cellulose were also detected, indicating that cellulose started to degrade.

We propose a qualitative model to explain the mechanism of cell wall thermal aging due to elevated temperatures (Figure 7). From the outside to inside, the surface layer of the wood cell wall is composed of extractives, the hemicellulose−lignin matrix, and the cellulose aggregates: the combination of these substances affected the adhesion force magnitude and jump-off force ratio in the force−displacement curve (Figure 2). The heat treatments accelerate the transport of extractives to the surface and their oxidation process; the transportation process prevails at 70 °C and the oxidation process dominates at 150 °C: the first sigmoidal curve (see Figure 4a). The extended heating at 150 °C degrades the amorphous hemicellulose−lignin matrix layer and exposes the cellulose aggregate layer with a pattern of parallel lines: the second sigmoidal curve (Figure 5a).

We attribute the first sigmoidal curve to the transportation and oxidation of extractives and the second sigmoidal curve to the degradation of the hemicellulose−lignin matrix. This conclusion is confirmed by the FTIR tests on the treated wood and the GC−MS tests on the volatiles during the heating of wood as well as by the literature.[36] For the second sigmoidal curve (Figure 5), our FTIR data cannot explain phases 1 and 2 separately: we can only suggest that the two phases indicate the degradation of the hemicellulose−lignin matrix. We infer that phase 2 results from hemicellulose degradation and phase 3 from the lignin—the literature shows that hemicelluloses degrade before lignin.[43]

CONCLUSIONS

Our study shows that AFM can be successfully used to measure the effect of temperatures on a lignocellulosic material. The key points are (1) a robust repositioning method to suppress the spatial variability of natural materials; (2) the combined interpretation of adhesion force magnitude, jump-off force ratio, and the topography; and (3) the consideration of the influence of extractives on the adhesion force measurements.

We found that the Boltzmann sigmoidal equation can describe the relationship between the adhesion force and jump-off force ratio in the thermal aging of wood surfaces. The first sigmoidal curve of the adhesion force−jump-off force ratio relationship describes the transportation of extractives and their oxidation on the surface. The second sigmoidal curve suggests the degradation of the hemicellulose−lignin matrix and the exposure of the cellulose aggregates. The adhesion force magnitude and the jump-off force ratio can be used to interpret the adhesion force measurements and the thermal aging of wood cell walls.

AUTHOR INFORMATION

Corresponding Authors

Juan Li − *Division of Organic and Wood-Based Materials, TU Braunschweig, 38102 Braunschweig, Germany;* orcid.org/0000-0001-6937-8296; Email: juan.li@tu-braunschweig.de

Bohumil Kasal − *Division of Organic and Wood-Based Materials, TU Braunschweig, 38102 Braunschweig, Germany; Fraunhofer Wilhelm-Klauditz-Institut WKI, 38108 Braunschweig, Germany*; Email: bohumil.kasal@wki.fraunhofer.de, kasalb@tu-bs.de

Complete contact information is available at: https://pubs.acs.org/10.1021/acs.biomac.1c01397

Author Contributions

J.L. designed the experiments, prepared the materials, and performed the experiments. J.L. analyzed the data and wrote the manuscript. B.K. directed the research and revised the manuscript.

Notes

The authors declare no competing financial interest.

ACKNOWLEDGMENTS

This research was partially funded by the German Research Foundation (DFG) as a part of the Graduiertenkolleg 2075. The Fraunhofer Wilhelm-Klauditz-Institute provided access to the AFM and FTIR equipment. The help of Martina Zühlke with nitrogen and Dr. Eric Uhde with the headspace GC−MS tests in the MAIC Department of the Fraunhofer Wilhelm-Klauditz-Institute is gratefully acknowledged.

REFERENCES

(1) Gillen, K. T.; Clough, R. L. Time-temperature-dose rate superposition: A methodology for extrapolating accelerated radiation aging data to low dose rate conditions. *Polym. Degrad. Stab.* **1989**, *24*, 137−168.

(2) Ding, H.-Z.; Wang, Z. D. Time−temperature superposition method for predicting the permanence of paper by extrapolating accelerated ageing data to ambient conditions. *Cellulose* **2007**, *14*, 171−181.

(3) Maiti, A.; Small, W.; Lewicki, J. P.; Weisgraber, T. H.; Duoss, E. B.; Chinn, S. C.; Pearson, M. A.; Spadaccini, C. M.; Maxwell, R. S.; Wilson, T. S. 3D printed cellular solid outperforms traditional stochastic foam in long-term mechanical response. *Sci. Rep.* **2016**, *6*, No. 24871.

(4) Tajvidi, M.; Falk, R. H.; Hermanson, J. C. Time-temperature superposition principle applied to a kenaf-fiber/high-density polyethylene composite. *J. Appl. Polym. Sci.* **2005**, *97*, 1995−2004.
(5) Zeniya, N.; Obataya, E.; Endo-Ujiie, K.; Matsuo-Ueda, M. Application of time−temperature−humidity superposition to the mass loss of wood through hygrothermally accelerated ageing at 95−140 °C and different relative humidity levels. *SN Appl. Sci.* **2019**, *1*, No. 3.
(6) Zheng, X. X.; Böttger, A. J.; Jansen, K. M. B.; van Turnhout, J.; van Kranendonk, J. Aging of Polyphenylene Sulfide-Glass Composite and Polysulfone in Highly Oxidative and Strong Alkaline Environments. *Front. Mater.* **2020**, *7*, No. 610440.
(7) Millett, M. A.; Gerhards, C. C. Accelerated aging: residual weight and flexural properties of wood heated in air at 115 °C to 175 °C. *Wood Sci.* **1972**, *4*, 193−201.
(8) Matsuo, M.; Yokoyama, M.; Umemura, K.; Gril, J.; Yano, K.; Kawai, S. Color changes in wood during heating: kinetic analysis by applying a time-temperature superposition method. *Appl. Phys. A* **2010**, *99*, 47−52.
(9) Sandberg, D.; Haller, P.; Navi, P. Thermo-hydro and thermo-hydro-mechanical wood processing: An opportunity for future environmentally friendly wood products. *Wood Mater. Sci. Eng.* **2013**, *8*, 64−88.
(10) Kránitz, K.; Sonderegger, W.; Bues, C.-T.; Niemz, P. Effects of aging on wood: a literature review. *Wood Sci Technol* **2016**, *50*, 7−22.
(11) Froidevaux, J.; Navi, P. Aging law of spruce wood. *Wood Mater. Sci. Eng.* **2013**, *8*, 46−52.
(12) Inagaki, T.; Mitsui, K.; Tsuchikawa, S. Near-infrared spectroscopic investigation of the hydrothermal degradation mechanism of wood as an analogue of archaeological objects. Part I: softwood. *Appl. Spectrosc.* **2008**, *62*, 1209−1215.
(13) Inagaki, T.; Siesler, H. W.; Mitsui, K.; Tsuchikawa, S. Difference of the crystal structure of cellulose in wood after hydrothermal and aging degradation: a NIR spectroscopy and XRD study. *Biomacromolecules* **2010**, *11*, 2300−2305.
(14) Ganne-Chédeville, C.; Jääskeläinen, A.-S.; Froidevaux, J.; Hughes, M.; Navi, P. Natural and artificial ageing of spruce wood as observed by FTIR-ATR and UVRR spectroscopy. *Holzforschung* **2012**, *66*, 163−170.
(15) Tsuchikawa, S.; Yonenobu, H.; Siesler, H. W. Near-infrared spectroscopic observation of the ageing process in archaeological wood using a deuterium exchange method. *Analyst* **2005**, *130*, 379−384.
(16) Wei, Y.; Zhang, P.; Liu, Y.; Chen, Y.; Gao, J.; Fan, Y. Kinetic Analysis of the Color of Larch Sapwood and Heartwood during Heat Treatment. *Forests* **2018**, *9*, No. 289.
(17) Casdorff, K.; Keplinger, T.; Burgert, I. Nano-mechanical characterization of the wood cell wall by AFM studies: comparison between AC- and QI mode. *Plant Methods* **2017**, *13*, No. 60.
(18) Fahlén, J.; Salmén, L. On the Lamellar Structure of the Tracheid Cell Wall. *Plant Biol.* **2002**, *4*, 339−345.
(19) Fahlén, J.; Salmén, L. Cross-sectional structure of the secondary wall of wood fibers as affected by processing. *J. Mater. Sci.* **2003**, *38*, 119−126.
(20) Fahlén, J.; Salmén, L. Pore and matrix distribution in the fiber wall revealed by atomic force microscopy and image analysis. *Biomacromolecules* **2005**, *6*, 433−438.
(21) Zimmermann, T.; Thommen, V.; Reimann, P.; Hug, H. J. Ultrastructural appearance of embedded and polished wood cell walls as revealed by Atomic Force Microscopy. *J. Struct. Biol.* **2006**, *156*, 363−369.
(22) Jin, X.; Kasal, B. Adhesion force mapping on wood by atomic force microscopy: influence of surface roughness and tip geometry. *R. Soc. Open Sci.* **2016**, *3*, No. 160248.
(23) Gusenbauer, C.; Jakob, D. S.; Xu, X. G.; Vezenov, D. V.; Cabane, É.; Konnerth, J. Nanoscale Chemical Features of the Natural Fibrous Material Wood. *Biomacromolecules* **2020**, *21*, 4244−4252.
(24) Frybort, S.; Obersriebnig, M.; Müller, U.; Gindl-Altmutter, W.; Konnerth, J. Variability in surface polarity of wood by means of AFM adhesion force mapping. *Colloids Surf., A* **2014**, *457*, 82−87.
(25) Meincken, M.; Evans, P. D. Nanoscale characterization of wood photodegradation using atomic force microscopy. *Eur. J. Wood Prod.* **2009**, *67*, 229−231.
(26) Mao, J.; Abushammala, H.; Kasal, B. Monitoring the surface aging of wood through its pits using atomic force microscopy with functionalized tips. *Colloids Surf., A* **2021**, *609*, No. 125871.
(27) Lagaňa, R.; Csiha, C.; Horváth, N.; Tolvaj, L.; Andor, T.; Kúdela, J.; Németh, R.; Kačík, F.; Ďurkovič, J. Surface properties of thermally treated European beech wood studied by PeakForce Tapping atomic force microscopy and Fourier-transform infrared spectroscopy. *Holzforschung* **2021**, *75*, 56−64.
(28) Li, J.; Kasal, B. Repeatability of Adhesion Force Measurement on Wood Longitudinal Cut Cell Wall Using Atomic Force Microscopy. *Wood Fiber Sci.* **2021**, *53*, 3−16.
(29) Cappella, B.; Dietler, G. Force-distance curves by atomic force microscopy. *Surf. Sci. Rep.* **1999**, *34*, 1−104.
(30) Landman, U.; Luedtke, W. D.; Burnham, N. A.; Colton, R. J. Atomistic mechanisms and dynamics of adhesion, nanoindentation, and fracture. *Science* **1990**, *248*, 454−461.
(31) Attard, P.; Parker, J. L. Deformation and adhesion of elastic bodies in contact. *Phys. Rev. A* **1992**, *46*, 7959−7971.
(32) Lynden-Bell, R. M. Computer simulations of fracture at the atomic level. *Science* **1994**, *263*, 1704−1705.
(33) Agraït, N.; Rubio, G.; Vieira, S. Plastic Deformation of Nanometer-Scale Gold Connective Necks. *Phys. Rev. Lett.* **1995**, *74*, 3995−3998.
(34) Weisenhorn, A. L.; Maivald, P.; Butt, H. J.; Hansma, P. K. Measuring adhesion, attraction, and repulsion between surfaces in liquids with an atomic-force microscope. *Phys. Rev. B: Condens. Matter Mater. Phys.* **1992**, *45*, 11226−11232.
(35) Safar, M.; Bertrand, D.; Robert, P.; Devaux, M. F.; Genot, C. Characterization of edible oils, butters and margarines by Fourier transform infrared spectroscopy with attenuated total reflectance. *J. Am. Oil Chem. Soc.* **1994**, *71*, 371−377.
(36) Nuopponen, M.; Vuorinen, T.; Jms, S.; Viitaniemi, P. The effects of a heat treatment on the behaviour of extractives in softwood studied by FTIR spectroscopic methods. *Wood Sci. Technol.* **2003**, *37*, 109−115.
(37) Green, D. W.; Evans, J. W.; Craig, B. A. Durability of structural lumber products at high temperatures. Part I, 66C at 75% RH and 82C at 30% RH. *Wood Fiber Sci.* **2003**, *35*, 499−523.
(38) Sevcik, C. Caveat on the Boltzmann distribution function use in biology. *Prog. Biophys. Mol. Biol.* **2017**, *127*, 33−42.
(39) El Aferni, A.; Guettari, M.; Tajouri, T. Mathematical model of Boltzmann's sigmoidal equation applicable to the spreading of the coronavirus (Covid-19) waves. *Environ. Sci. Pollut. Res.* **2021**, *28*, 40400−40408.
(40) Penttilä, P. A.; Altgen, M.; Awais, M.; Österberg, M.; Rautkari, L.; Schweins, R. Bundling of cellulose microfibrils in native and polyethylene glycol-containing wood cell walls revealed by small-angle neutron scattering. *Sci. Rep.* **2020**, *10*, No. 20844.
(41) Sikora, A.; Kačík, F.; Gaff, M.; Vondrová, V.; Bubeníková, T.; Kubovský, I. Impact of thermal modification on color and chemical changes of spruce and oak wood. *J. Wood Sci.* **2018**, *64*, 406−416.
(42) González-Peña, M. M.; Curling, S. F.; Hale, M. D. On the effect of heat on the chemical composition and dimensions of thermally-modified wood. *Polym. Degrad. Stab.* **2009**, *94*, 2184−2193.
(43) Esteves, B.; Velez Marques, A.; Domingos, I.; Pereira, H. Chemical changes of heat treated pine and eucalypt wood monitored by FTIR. *Maderas: Cienc. Tecnol.* **2013**, *15*, 245−258.
(44) Li, J.; Li, B.; Zhang, X. Comparative studies of thermal degradation between larch lignin and manchurian ash lignin. *Polym. Degrad. Stab.* **2002**, *78*, 279−285.
(45) Kubovský, I.; Kačíková, D.; Kačík, F. Structural Changes of Oak Wood Main Components Caused by Thermal Modification. *Polymers* **2020**, *12*, No. 485.
(46) Tjeerdsma, B. F.; Militz, H. Chemical changes in hydrothermal treated wood: FTIR analysis of combined hydrothermal and dry heat-treated wood. *Eur. J. Wood Prod.* **2005**, *63*, 102−111.

https://doi.org/10.1021/acs.biomac.1c01397
Biomacromolecules 2022, 23, 1601−1609

(47) Popescu, M.-C.; Froidevaux, J.; Navi, P.; Popescu, C.-M. Structural modifications of Tilia cordata wood during heat treatment investigated by FT-IR and 2D IR correlation spectroscopy. *J. Mol. Struct.* **2013**, *1033*, 176−186.
(48) Carrier, M.; Fournet, R.; Sirjean, B.; et al. Fast Pyrolysis of Hemicelluloses into Short-Chain Acids: An Investigation on Concerted Mechanisms. *Energy Fuels* **2020**, *34*, 14232−14248.
(49) Riyadi, F. A.; Tahir, A. A.; Yusof, N.; Sabri, N. S. A.; Noor, M. J. M. M.; Akhir, F. N. M. D.; Othman, N.; Zakaria, Z.; Hara, H. Enzymatic and genetic characterization of lignin depolymerization by Streptomyces sp. S6 isolated from a tropical environment. *Sci. Rep.* **2020**, *10*, No. 7813.
(50) Wang, Z.; Lu, Q.; Zhu, X.-F.; Zhang, Y. Catalytic fast pyrolysis of cellulose to prepare levoglucosenone using sulfated zirconia. *ChemSusChem* **2011**, *4*, 79−84.
(51) Wang, Z.; Lu, Q.; Zhu, X.-F.; Zhang, Y. Catalytic fast pyrolysis of cellulose to prepare levoglucosenone using sulfated zirconia. *ChemSusChem* **2011**, *4* (1), 79−84.
(52) Kačík, F.; Veľková, V.; Šmíra, P.; Nasswettrová, A.; Kačíková, D.; Reinprecht, L. Release of terpenes from fir wood during its long-term use and in thermal treatment. *Molecules (Basel, Switzerland)* **2012**, *17* (8), 9990−9999.

https://doi.org/10.1021/acs.biomac.1c01397
Biomacromolecules 2022, 23, 1601−1609